# Indium incorporation and emission properties of nonpolar and semipolar InGaN quantum wells

Yuji Zhao,[1,a)] Qimin Yan,[2] Chia-Yen Huang,[2] Shih-Chieh Huang,[2] Po Shan Hsu,[2] Shinichi Tanaka,[2] Chih-Chien Pan,[2] Yoshinobu Kawaguchi,[2] Kenji Fujito,[3] Chris G. Van de Walle,[2] James S. Speck,[2] Steven P. DenBaars,[1,2] Shuji Nakamura,[1,2] and Daniel Feezell[2]
[1]*Electrical and Computer Engineering Department, University of California, Santa Barbara, California 93106, USA*
[2]*Materials Department, University of California, Santa Barbara, California 93106, USA*
[3]*Optoelectronic Laboratory, Mitsubishi Chemical Corporation, 1000 Higashi-Mamiana, Ushiku, Ibaraki 300-1295, Japan*

(Received 7 April 2012; accepted 3 May 2012; published online 16 May 2012)

We report indium incorporation properties on various nonpolar and semipolar free-standing GaN substrates. Electroluminescence characterization and x-ray diffraction (XRD) analysis indicate that the semipolar $(20\bar{2}\bar{1})$ and $(11\bar{2}2)$ planes have the highest indium incorporation rate among the studied planes. We also show that both indium composition and polarization-related electric fields impact the emission wavelength of the quantum wells (QWs). The different magnitudes and directions of the polarization-related electric fields for each orientation result in different potential profiles for the various semipolar and nonpolar QWs, leading to different emission wavelengths at a given indium composition. © *2012 American Institute of Physics*. [http://dx.doi.org/10.1063/1.4719100]

Nonpolar and semipolar III-nitrides have been extensively investigated as possible substrates for the growth of high-indium-content quantum wells (QWs) in green light-emitting diodes (LEDs) and laser diodes (LDs).[1–4] One advantage of nonpolar and semipolar growth is the elimination or reduction of polarization-related electric fields in the QW, which are responsible for the reduced radiative recombination rate and large blue shift observed in conventional *c*-plane emitters.[5–7] The issues associated with polarization-related electric fields are exacerbated for higher indium content QWs. Consequently, the nonpolar *m*-plane orientation was initially considered a promising candidate for longer wavelength LEDs (Ref. 8) and LDs.[9] However, the reported stimulated emission wavelength for *m*-plane LDs has been limited to around 500 nm.[10] Challenges associated with indium incorporation and related defect formation[11] have made it difficult to grow high-quality QWs with high indium composition on *m*-plane.

Alternatively, select semipolar planes have been shown theoretically and experimentally to exhibit high indium incorporation. For example, the semipolar $(11\bar{2}2)$ plane was reported to have binding sites that may accommodate indium atoms more easily than either *c*-plane or *m*-plane.[12] Additionally, long wavelength yellow LEDs have been demonstrated on this plane.[13] However, the formation of misfit dislocations (MDs) within the active region has been observed and is known to degrade the device performance.[14] The semipolar $(20\bar{2}1)$ plane, which is miscut by 15° toward *c*-plane from *m*-plane, has been utilized to produce high-performance green LEDs (Refs. 15 and 16) and LDs.[3,4] More recently, several advantageous features, including high optical polarization ratio, small wavelength shift, and low efficiency droop, were reported on blue-green $(20\bar{2}\bar{1})$ LEDs (Refs. 17 and 18) and LDs.[19] However, there are very few reports of the indium incorporation on these orientations. In this paper, we compare the indium incorporation on nonpolar *m*-plane and several semipolar planes, including $(20\bar{2}1)$, $(20\bar{2}\bar{1})$, $(30\bar{3}1)$, $(30\bar{3}\bar{1})$, and $(11\bar{2}2)$. The inclination angles from *m*-plane are 32° for $(11\bar{2}2)$, 15° for $(20\bar{2}1)$ and $(20\bar{2}\bar{1})$ (toward $+c$ and $-c$, respectively), and 10° for $(30\bar{3}1)$ and $(30\bar{3}\bar{1})$ (toward $+c$ and $-c$, respectively). In addition, we discuss the impacts of indium composition and polarization-related electric fields on the emission wavelengths of nonpolar and semipolar devices.

LED structures were homoepitaxially grown by conventional metal organic chemical vapor deposition (MOCVD) on free-standing GaN substrates supplied by Mitsubishi Chemical Corporation. All the semipolar and nonpolar GaN substrates have a thickness of 330 $\mu$m. The InGaN growth rate was verified to be the same for the various semipolar and nonpolar planes by superlattice x-ray diffraction (XRD) analysis. The device structure consisted of a 1 $\mu$m Si-doped *n*-type GaN layer, an InGaN (3 nm) single quantum well (SQW) active region, a 16 nm Mg-doped $Al_{0.15}Ga_{0.85}N$ electron blocking layer (EBL), and a 60 nm *p*-type GaN layer. To study the different indium incorporation rates between nonpolar and semipolar planes, two series of experiments were performed. Samples with different substrate orientations were co-loaded in the MOCVD reactor to ensure identical epitaxial growth conditions. Electroluminescence (EL) measurements indicate that all the LED samples have comparable light-output-powers. In the first series, SQW LED structures were grown on $(20\bar{2}\bar{1})$, $(20\bar{2}1)$, $(30\bar{3}\bar{1})$, $(30\bar{3}1)$, and *m*-plane GaN at the same growth temperature (780 °C), while the trimethylindium (TMI) flow was varied from 85 to 105 sccm. The resulting EL wavelengths for the first series are summarized in Fig. 1(a) and schematic views of the nonpolar and semipolar planes that were examined are shown in the inset. In general, devices grown on planes with higher inclination angles from the *m*-plane exhibited longer emission wavelengths than those on less-inclined planes. These results are consistent with previously published simulations that

[a)]E-mail: yujizhao@engineering.ucsb.edu.

 

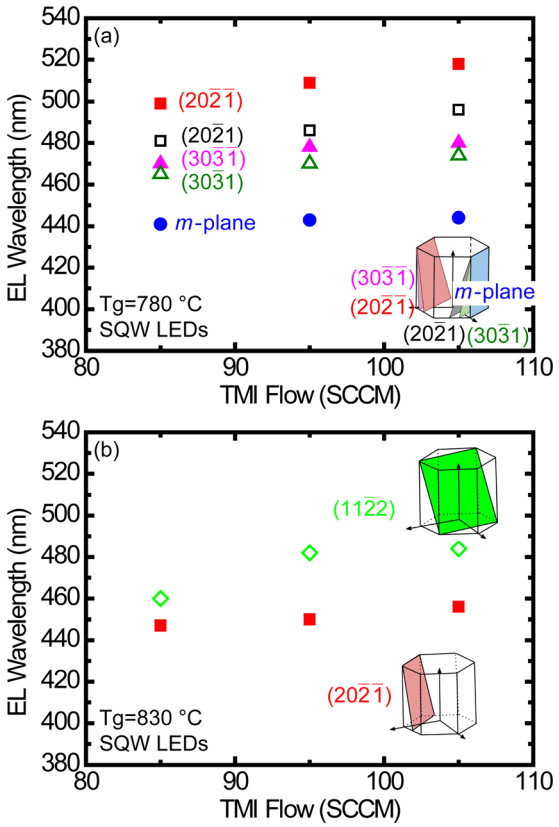


FIG. 1. EL peak wavelength as a function of TMI flow for SQW LEDs (a) on $(20\bar{2}\bar{1})$, $(20\bar{2}1)$, $(30\bar{3}\bar{1})$, $(30\bar{3}1)$, and *m*-planes at a growth temperature of 780 °C and (b) on $(20\bar{2}\bar{1})$ and $(11\bar{2}2)$ planes at a growth temperature of 830 °C. Insets: schematic views of the relevant nonpolar and semipolar planes in the wurtzite crystal structure.

predicted high indium incorporation on semipolar surfaces due to the reduction of the strain-induced repulsive interaction between incorporated indium atoms.[20] However, previous analysis did not considered planes with the same inclination angle and opposite surface polarities. In our experiments, although characterized by identical strain conditions,[21] the semipolar $(20\bar{2}\bar{1})$ plane (Ga-polar character) consistently exhibited higher indium incorporation than the opposite semipolar $(20\bar{2}1)$ plane (N-polar character) (see Table I). Similar results were also observed on the $(30\bar{3}\bar{1})$ and $(30\bar{3}1)$ planes.[22] Previous reports have indicated that Ga- and N-polar *c*-plane surfaces exhibit different indium incorporation rates, indicating that surface chemistry is expected to affect the indium incorporation properties.[23]

Separately, the co-loaded experiment described above was performed to compare the semipolar $(20\bar{2}\bar{1})$ and $(11\bar{2}2)$ planes at a growth temperature of 830 °C. A higher growth temperature was necessary for this experiment to avoid stress relaxation in the $(11\bar{2}2)$ samples. The resulting EL wavelengths are shown in Fig. 1(b) and schematic views of the $(20\bar{2}\bar{1})$ and $(11\bar{2}2)$ planes are presented as insets. Devices on the $(11\bar{2}2)$ plane (32° from *m*-plane) exhibited longer emission wavelengths than those on the $(20\bar{2}\bar{1})$ plane (15° from *m*-plane). However, due to the larger resolved shear stresses on the $(11\bar{2}2)$ plane, MDs easily form at the hetero-interfaces via the available slip system on the (0001) basal plane. This is problematic for hetero-structures grown with large lattice mismatches.[14] The $(20\bar{2}\bar{1})$ plane, on the other hand, has a larger critical thickness than the $(11\bar{2}2)$ plane, which allows for the growth of thicker coherent layers.[24]

In the second series, $(20\bar{2}\bar{1})$ and $(20\bar{2}1)$ wafers were co-loaded with a fixed TMI flow (160 sccm) in the SQW and the InGaN growth temperature was varied from 820 °C to 920 °C. The results of the EL wavelengths of this series are summarized in Fig. 2. The $(20\bar{2}\bar{1})$ SQW devices exhibited longer emission wavelengths compared to the co-loaded $(20\bar{2}1)$ devices for all temperatures that were examined. Since indium incorporation in GaN strongly depends on growth temperature, $(20\bar{2}\bar{1})$ InGaN QWs can be grown at a higher temperature (30 to 50 °C higher) than $(20\bar{2}1)$ QWs for the same emission wavelength, which may contribute to higher crystal quality and/or reduced indium or thickness fluctuations for QWs on the $(20\bar{2}\bar{1})$ plane.

Since the measured EL emission wavelength depends upon indium composition and polarization-related electric fields (i.e.,—QW shape), XRD analysis was performed to decouple the two effects. The samples studied in the XRD experiments were comprised of two series of structures. In the first series, LED structures with 3 pairs of InGaN (3 nm)/GaN (10 nm) QWs were grown on $(20\bar{2}\bar{1})$, $(20\bar{2}1)$, $(11\bar{2}2)$, and *m*-plane in a co-loaded experiment and characterized by XRD analysis. Cathodoluminescence (CL) and XRD experiments confirmed that all the structures were coherently strained. The EL emission wavelengths, photoluminescence (PL) emission wavelengths, and the indium compositions extracted from XRD for each sample are summarized in Table I. The indium compositions on the $(11\bar{2}2)$ plane (24.6%) and the $(20\bar{2}\bar{1})$ plane (24.1%) were significantly higher than those on the $(20\bar{2}1)$ plane (17.3%) and the

TABLE I. EL wavelength, PL wavelength, and indium composition for co-loaded *m*-plane, $(20\bar{2}1)$, $(20\bar{2}\bar{1})$, and $(11\bar{2}2)$ LEDs with 3 sets of InGaN/GaN QWs.

| Substrate orientations | EL wavelength (nm) | PL wavelength (nm) | In composition (%) |
|---|---|---|---|
| *m*-plane | 415 | 415 | 15.7 |
| $(20\bar{2}1)$ | 438 | 434 | 17.3 |
| $(20\bar{2}\bar{1})$ | 470 | 467 | 24.1 |
| $(11\bar{2}2)$ | 490 | 485 | 24.6 |

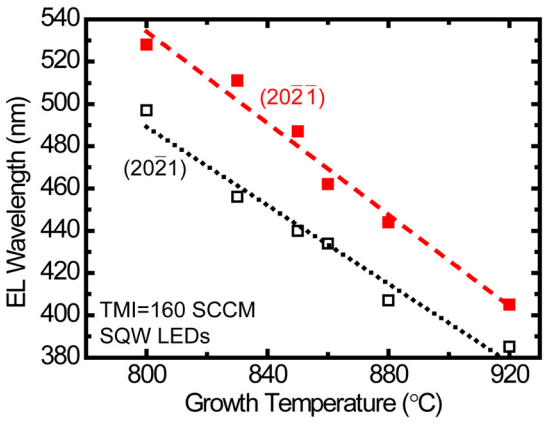


FIG. 2. EL peak wavelength as a function of growth temperature for SQW LEDs on the $(20\bar{2}\bar{1})$ and $(20\bar{2}1)$ planes at a TMI flow of 160 SCCM.

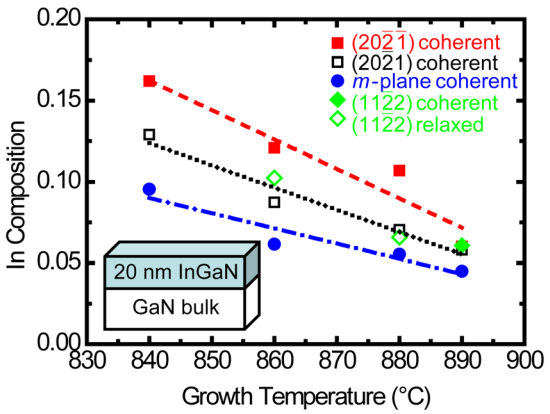


FIG. 3. Measured indium incorporation as a function of growth temperature for co-loaded InGaN films of 20 nm on $(20\bar{2}\bar{1})$, $(20\bar{2}1)$, $(11\bar{2}2)$, and *m*-plane. Inset: schematic view of the sample structure.

*m*-plane (15.7%), which is consistent with previous findings. The indium compositions are in reasonable agreement with the EL and PL wavelengths. In the second series, InGaN films with a thickness of 20 nm were grown on co-loaded $(20\bar{2}\bar{1})$, $(20\bar{2}1)$, $(11\bar{2}2)$, and *m*-plane GaN substrates under different temperatures (840 °C to 890 °C). The indium compositions of the samples were determined by XRD and are presented in Fig. 3. All the films were coherently strained, as verified by CL and XRD, with the exception of the $(11\bar{2}2)$ films at 860 °C and 880 °C. The $(20\bar{2}\bar{1})$ samples again showed higher indium compositions compared with the $(20\bar{2}1)$ and *m*-plane samples. Under high growth temperatures (890 °C), the $(11\bar{2}2)$ samples were coherent and showed similar indium compositions to the $(20\bar{2}\bar{1})$ samples. However, under lower growth temperatures (840 to 880 °C), the $(11\bar{2}2)$ samples were stress relaxed via formation of basal plane MDs at the heterointerfaces.[14] The indium composition of stress relaxed samples were estimated using symmetric reciprocal space maps with the x-ray beam oriented along the *c*-azimuth.[24] The defected $(11\bar{2}2)$ samples were estimated to have lower indium compositions compared to the coherent $(20\bar{2}\bar{1})$ samples, but the effect of stress relaxation and related defects on the indium incorporation is not yet clear and is a topic of ongoing investigation.

Although similar indium compositions were extracted for the coherent structures on the $(20\bar{2}\bar{1})$ plane and the $(11\bar{2}2)$ plane, those on the $(11\bar{2}2)$ plane exhibited longer emission wavelengths. Similar results were also observed when comparing the *m*-plane and the $(20\bar{2}1)$ plane, with $(20\bar{2}1)$ exhibiting longer emission wavelengths. These results are qualitatively explained by the different magnitudes and directions of polarization-related electric fields in the QWs on the different planes, which lead to various degrees of band-bending in the QWs. To fully clarify this phenomenon, simulations for blue-green LED structures were carried out using the commercial SIMULED package developed by the STR Group.[25] The potential distributions were calculated by solving the Schrodinger-Poisson equations self-consistently and include strain and polarization effects. The strain and piezoelectric polarization charges in the nonpolar and semipolar heterostructures are calculated with the approach used in Ref. 21. The piezoelectric constants for InN, GaN, and AlN are taken from Refs. 26–28, while the spontaneous polarization constants are taken from Ref. 29. For simple interpretation, identical SQW LED structures (with 25% indium composition) were simulated under a current density of 20 A/cm$^2$. The calculated band diagrams and peak emission wavelengths for $(20\bar{2}\bar{1})$, $(20\bar{2}1)$, $(11\bar{2}2)$ and *m*-plane devices are shown in Figs. 3(a)–3(d). For a given indium composition, the emission wavelengths of $(20\bar{2}1)$ and $(11\bar{2}2)$ LEDs were approximately 10–15 nm longer than those of the $(20\bar{2}\bar{1})$ and *m*-plane LEDs. Again, these differences are explained by the magnitudes and directions of polarization-related electric fields in the QWs. For the $(20\bar{2}1)$ and $(11\bar{2}2)$ planes, the polarization-related electric field in the QWs is in the same direction as the *p-n* junction built-in electric field. For the $(20\bar{2}\bar{1})$ plane, the polarization-related electric field opposes the *p-n* junction built-in electric field. For the *m*-plane, the polarization-related electric field is zero, and only the *p-n* junction built-in electric field exists in the QWs (in the unbiased case). As a result, distinct potential profiles are obtained in the QWs of $(20\bar{2}\bar{1})$, $(20\bar{2}1)$, $(11\bar{2}2)$ and *m*-plane devices. At a low current density (20 A/cm$^2$), InGaN QWs on the $(20\bar{2}1)$ and $(11\bar{2}2)$ planes exhibit triangular potential profiles, since the polarization-related electric field and the *p-n* junction built-in electric field are additive (Fig. 4). Conversely, QWs on the $(20\bar{2}\bar{1})$ plane exhibit relatively flat potential profiles, since the polarization-related electric field and the *p-n* junction built-in electric field are opposite in direction and nearly equal in magnitude. *m*-plane QWs also exhibit relatively flat potential profiles beyond diode turn-on. Triangular potential profiles produce a red shift in the emission and contribute to the longer emission wavelengths observed on $(20\bar{2}1)$ and $(11\bar{2}2)$ compared to *m*-plane and $(20\bar{2}\bar{1})$, respectively, for a given indium composition. However, the red shift at low current densities in $(20\bar{2}1)$ and $(11\bar{2}2)$ QWs is counteracted at larger current densities by carrier-induced screening of the electric fields. The cumulative result is a blue shift of the emission wavelength with increasing current, which is problematic for achieving wavelength stable LEDs and LDs.[30] Conversely, LEDs on $(20\bar{2}\bar{1})$ show very little blue shift.[19]

In summary, we compared the indium incorporation on various nonpolar and semipolar planes. Among the planes examined, the semipolar $(11\bar{2}2)$ and $(20\bar{2}\bar{1})$ planes exhibited the highest indium incorporation. As a result, we found that QWs on semipolar $(20\bar{2}\bar{1})$ can be grown at significantly higher temperatures compared to those on semipolar $(20\bar{2}1)$ for the same emission wavelength. Furthermore, we demonstrated that both the indium composition and the magnitude and direction of the polarization-related electric fields in the QWs impact the emission wavelength. For planes on which the polarization-related electric field and the *p-n* junction built-in electric field are additive (e.g.,—$(11\bar{2}2)$ and $(20\bar{2}1)$), a triangular potential profile results in the QWs and a red shift in the emission wavelength is obtained, resulting in a blue shift with increasing current injection. For some planes on which the polarization-related electric field and the *p-n* junction built-in electric field are subtractive (e.g.,—$(20\bar{2}\bar{1})$), a relatively flat potential profile can be obtained, which leads to a shorter emission wavelength for a given indium composition, but nearly completely eliminates blue shift.

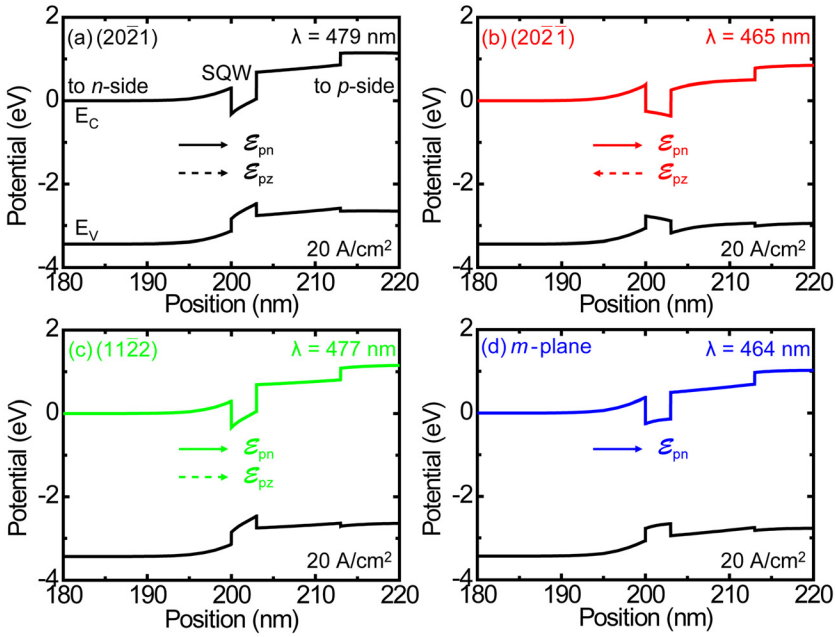


FIG. 4. Simulated band diagrams and emission wavelengths for SQW (with 25% indium composition) blue-green LEDs on the (a) (20$\bar{2}$1), (b) (20$\bar{2}\bar{1}$), (c) (11$\bar{2}$2), and (d) *m*-planes at a current density of 20 mA/cm$^2$.

Y. Zhao would like to thank Matthew T. Hardy and Erin C. Young for the helpful discussion of XRD analysis. The authors acknowledge the support of Solid State Lighting and Energy Center at UCSB. A portion of this work was done in the UCSB nanofabrication facility, part of the NSF funded NNIN. This work made use of MRL Central Facilities supported by the MRSEC Program of the National Science Foundation under Award No. DMR05-20415.

[1]S. Nakamura, MRS Bull. **34**, 101 (2009).
[2]J. W. Raring, M. C. Schmidt, C. Poblenz, Y. C. Chang, M. J. Mondry, B. Li, J. Iveland, B. Walters, M. R. Krames, R. Craig, P. Rudy, J. S. Speck, S. P. DenBaars, and S. Nakamura, Appl. Phys. Express **3**, 112101 (2010).
[3]Y. Enya, Y. Yoshizumi, T. Kyono, K. Akita, M. Ueno, M. Adachi, T. Sumitomo, S. Tokuyama, T. Ikegami, K. Katayama, and T. Nakamura, Appl. Phys. Express **2**, 082101 (2009).
[4]Y. D. Lin, S. Yamamoto, C. Y. Huang, C. L. Hsiung, F. Wu, K. Fujito, H. Ohta, J. S. Speck, S. P. Denbaars, and S. Nakamura, Appl. Phys. Express **3**, 082001 (2010).
[5]P. Waltereit, O. Brandt, A. Trampert, H. T. Grahn, J. Menniger, M. Ramsteiner, M. Reiche, and K. H. Ploog, Nature (London) **406**, 865 (2000).
[6]F. Bernardini and V. Fiorentini, Phys. Status Solidi B **216**, 391 (1999).
[7]M. C. Schmidt, K. C. Kim, H. Sato, N. Fellows, H. Masui, S. Nakamura, S. P. DenBaars, and J. S. Speck, Jpn. J. Appl. Phys., Part 2 **46**, L126 (2007).
[8]Y. D. Lin, A. Chakraborty, S. Brinkley, H. C. Kuo, T. Melo, K. Fujito, J. S. Speck, S. P. DenBaars, and S. Nakamura, Appl. Phys. Lett. **94**, 261108 (2009).
[9]Y. D. Lin, M. T. Hardy, P. S. Hsu, K. M. Kelchner, C. Y. Huang, D. A. Haeger, R. M. Farrell, K. Fujito, A. Chakraborty, H. Ohta, J. S. Speck, S. P. DenBaars, and S. Nakamura, Appl. Phys. Express **2**, 082102 (2009).
[10]K. Okamoto, J. Kashiwagi, T. Tanaka, and M. Kubota, Appl. Phys. Lett. **94**, 071105 (2009).
[11]F. Wu, Y. D. Lin, A. Chakraborty, H. Ohta, S. P. DenBaars, S. Nakamura, and J. S. Speck, Appl. Phys. Lett. **96**, 231912 (2010).
[12]J. E. Northrup, Appl. Phys. Lett. **95**, 133107 (2009).
[13]H. Sato, R. B. Chung, H. Hirasawa, N. Fellows, H. Masui, F. Wu, M. Saito, K. Fujito, J. S. Speck, S. P. DenBaars, and S. Nakamura, Appl. Phys. Lett. **92**, 221110 (2008).
[14]P. S. Hsu, E. C. Young, A. E. Romanov, K. Fujito, S. P. DenBaars, S. Nakamura, and J. S. Speck, Appl. Phys. Lett. **99**, 081912 (2011).
[15]T. Kyono, Y. Yoshizumi, Y. Enya, M. Adachi, S. Tokuyama, M. Ueno, K. Katayama, and T. Nakamura, Appl. Phys. Express **3**, 011003 (2010).
[16]S. Yamamoto, Y. Zhao, C. C. Pan, R. B. Chung, K. Fujito, J. Sonoda, S. P. Denbaars, and S. Nakamura, Appl. Phys. Express **3**, 122102 (2010).
[17]Y. Zhao, T. Tanaka, Q. Yan, C. Y. Huang, R. B. Chung, C. C. Pan, K. Fujito, D. Feezell, C. G. Van de Walle, J. S. Speck, S. P. DenBaars, and S. Nakamura, Appl. Phys. Lett. **99**, 051109 (2011).
[18]Y. Zhao, S. Tanaka, C. C. Pan, K. Fujito, D. Feezell, J. S. Speck, S. P. DenBaars, and S. Nakamura, Appl. Phys. Express **4**, 082104 (2011).
[19]C. Y. Huang, M. T. Hardy, K. Fujito, D. Feezell, J. S. Speck, S. P. DenBaars, and S. Nakamura, Appl. Phys. Lett. **95**, 241115 (2011).
[20]M. V. Durnev, A. V. Omelchenko, E. V. Yakovlev, I. Yu. Evstratov, and S. Yu. Karpov, Appl. Phys. Lett. **97**, 051904 (2010).
[21]A. E. Romanov, T. J. Baker, S. Nakamura, and J. S. Speck, J. Appl. Phys. **100**, 023522 (2006).
[22]P. S. Hsu, J. Sonoda, K. M. Kelchner, A. Tyagi, R. M. Farrell, D. A. Haeger, E. C. Young, A. E. Romanov, K. Fujito, H. Ohta, S. P. DenBaars, J. S. Speck, and S. Nakamura, Phys. Status Solidi C **8**, 2390 (2011).
[23]S. Keller, N. A. Fichtenbaum, M. Furukawa, J. S. Speck, S. P. DenBaars, and U. K. Mishra, Appl. Phys. Lett. **90**, 191908 (2007).
[24]E. C. Young, C. S. Gallinat, A. E. Romanov, A. Tyagi, F. Wu, and J. S. Speck, Appl. Phys. Express **3**, 111002 (2010).
[25]V. F. Mymrin, K. A. Bulashevich, N. I. Podolskaya, I. A. Zhmakin, S. Yu. Karpov, and Yu. N. Makarov, Phys. Status Solidi C **2**, 2928 (2005).
[26]J. G. Gualtieri, J. A. Kosinski, and A. Ballato, IEEE Trans. Ultrason. Ferroelectr. Freq. Control **41**, 53 (1994).
[27]A. E. Romanov, P. Waltereit, and J. S. Speck, J. Appl. Phys. **97**, 043708 (2005).
[28]S. Nakamura, S. Pearton, and G. Fasol, *The Blue Laser Diode: The Complete Story*, 2nd ed. (Springer, Berlin, 2000).
[29]F. Bernardini, V. Fiorentini, and D. Vanderbilt, Phys. Rev. B **56**, R10024 (1997).
[30]M. H. Crawford, IEEE J. Sel. Top. Quantum Electron. **15**, 1028 (2009).